

L Band Radar Backscatter Dependence Upon Surface Wind Stress: A Summary of New SEASAT-1 and Aircraft Observations

T. W. THOMPSON

*Planetary Science Institute, Science Applications, Inc., Pasadena, California 91101 and
Jet Propulsion Laboratory, Telecommunications Science and Engineering Division, Pasadena, California 91109*

D. E. WEISSMAN

Hofstra University, Department of Engineering Science, Hempstead, New York 11550

F. I. GONZALEZ

National Oceanic and Atmospheric Administration/Pacific Marine Environment Laboratory, Seattle, Washington 98105

Radar backscatter from the ocean depends on surface wind stress for a wide range of radar wavelengths. Here, we have reviewed the wind-radar relationships for *L* band radar wavelengths near 25 cm and 20° angle of incidence and HH polarization using a number of aircraft and SEASAT-1 SAR observations. At this wavelength, the *L* band backscatter coefficient (σ^0) from the ocean appears to depend upon surface wind speed ($|\bar{U}|$) and direction (ϕ) in the following manner: $\sigma^0 = K|\bar{U}|^a [1 + b \cos(2\phi)]$. The wind-speed coefficient a is 0.5 ± 0.1 for a wide range of wind speeds. The wind-direction coefficient b is near zero (i.e., $b = 0.05 \pm 0.05$) for lower winds and stable marine boundary layers. However, one unusual aircraft observation suggests that $b = 0.20 \pm 0.05$ for moderate wind speeds and an unstable marine boundary layer. We have examined a variety of aircraft and SEASAT-1 observations. SEASAT synthetic aperture radar (SAR) observations in conjunction with simultaneous SEASAT scatterometer measurements provide an excellent measurement of the wind-speed coefficient a since a variety of wind speeds can be observed in a few minutes. Aircraft observations provide an excellent measurement of the wind-direction coefficient b since a number of directions can be examined in about 1 hour with special flight patterns designed for multiple look directions. Thus, both aircraft and spacecraft observations were studied in this work. We have interpreted these aircraft and spacecraft results in terms of existing theoretical models for radar scattering from the ocean. We believe that modulation of echo power by the magnitude of the wind occurs through both large-scale slope effects as well as through growth of the short gravity wave-height spectrum. Our data is near an angle of incidence of 20° where a two scale scattering model must be used.

INTRODUCTION

Recent radar research inspired by the SEASAT-1 mission has been directed toward (1) understanding electromagnetic scattering from the ocean and (2) applying this knowledge to monitoring the ocean surface and studying air-sea interactions. There is a new and rapidly expanding interest in continuing this exploration, and the data base recently acquired from many aircraft missions and the SEASAT mission is being actively investigated to assess how well meteorological and oceanographic variables can be measured by radar.

In the past 15 years, radar observations of the ocean have indicated that the strength of radar echoes are related to surface stress. The pioneering work reported by Daley [1973] was conducted by Naval Research Laboratory (NRL) personnel in the late 1960's with aircraft observations using a four-frequency radar. Further analysis of this NRL aircraft data by Jones and Schroder [1978] and Skylab spacecraft observations led to the SEASAT-1 spacecraft radar scatterometers which measured surface wind speeds and directions [see Bracalente et al., 1980; Johnson et al., 1980]. These spacecraft radars operate at K_u band frequencies of 13.9 GHz with radar wavelengths of 2.2 cm. The spacecraft

observations and theory [Moore and Fung, 1979; Barrick and Swift, 1980] suggest that radar backscatter and surface wind speed and direction have the following relationship:

$$\sigma^0 = K|\bar{U}|^a [1 + b \cos(2\phi) + c \cos(\phi)] \quad (1)$$

where σ^0 = radar backscatter coefficient, $|\bar{U}|$ = wind-speed magnitude, ϕ = wind-radar angle, a = wind-speed coefficient, b and c = wind-direction coefficients, and K = backscattered power coefficient.

The wind-radar angle is defined such that $\phi = 0$ when the radar's line-of-sight propagation is in the direction of the wind. Angle ϕ is $\pm 90^\circ$ when the radar is looking crosswind and ϕ is 180° when the wind is blowing toward the radar. The coefficient K depends upon the angle of incidence, the angle between the radar's line-of-sight propagation vector, and the normal to the surface.

Radar scatterometers at K_u band frequencies and higher (near 50° angles of incidence) indicate that $a = 1.75 = 0.25$ and $b = 0.30 = 0.05$. The a coefficient at the K_u band frequencies for lower angles of incidence is near unity. The wind direction coefficient c is smaller than b , and its value is subject to debate at this time. These coefficients are large enough to provide measurable differences in radar echo strength which, in turn, can be related to surface wind speed and direction.

The original NRL aircraft observations as well as a number of recent aircraft and SEASAT-1 observations sug-

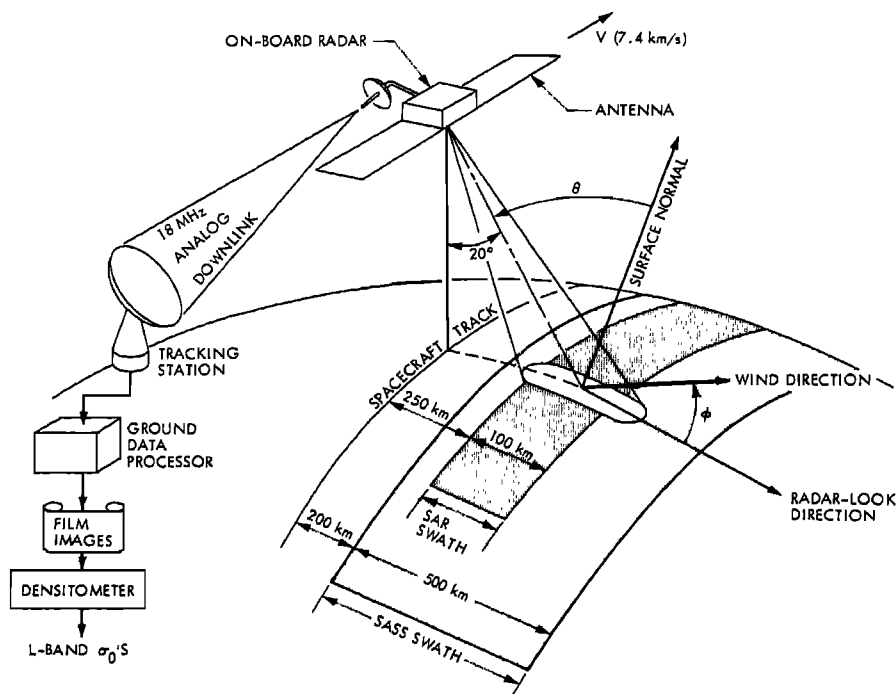


Fig. 1. Geometry for SEASAT SAR-scatterometer (SASS) observations of surface winds. Important radar geometric parameters include ϕ , the wind-radar angle (measured on the surface), and θ , the angle of incidence (the angle between the surface normal and the radar's line of sight). The SEASAT SAR antenna had a $1^\circ \times 5^\circ$ beam width; its footprint moved over the ocean surface at about 6.6 km/s.

gest radar backscatter from the ocean at L band frequencies has a similar relationship to surface wind speed and direction. The recent L band data are at radar wavelengths near 25 cm, about 10 times the K_u band wavelength. Recent aircraft observations of the Gulf Stream and Hurricane Gloria were reported by Weissman and Thompson [1977] and Weissman *et al.* [1979, 1980]. These were augmented by a number of SEASAT-1 observations reported by Beal [1979], Thompson *et al.* [1981], Ross [1981], Jones *et al.* [1981] and others.

We have tested the wind-radar relationship described above with a number of aircraft and SEASAT-1 observations. SEASAT-1 observations provide a measurement of

radar cross section versus wind-field scatterometer winds where a variety of wind speeds can be examined in a few minutes. These measurements usually do not provide a good measurement of the wind direction coefficient since wind directions often were in the same general direction with respect to the radar line-of-sight. To measure this wind-direction effect, we reexamined aircraft observations obtained during the Marineland Experiment [Thompson *et al.*, 1982]. Here, the aircraft flew over the same surface site in five or eight different directions in a few tens of minutes. These observations provide our best estimates of the wind-direction coefficient b . All of the work reported here has been conducted at an angle of incidence near 20° where the

TABLE 1. Radar Parameters for SEASAT-A Synthetic Aperture Radar (SAR)

Parameter	Value
Frequency	1274.8 MHz
Wavelength	23.5 cm
Antenna beamwidth, elevation	6 deg
Antenna beamwidth, azimuth	1 deg
Antenna beam center gain	34 db
Antenna pointing angle	20 degrees off nadir, right side
Angle of incidence	20° – 26°
Surface resolution (optical images)	$40 \text{ m} \times 40 \text{ m}$
Image swath width	100 km
Image length	up to 4000 km
Nominal altitude	800 km
Densitometer spot in image	1 mm circular
Densitometer spot on surface	500 m circular
Densitometer spot spacing	12.5 km across swath 66.0 km along swath

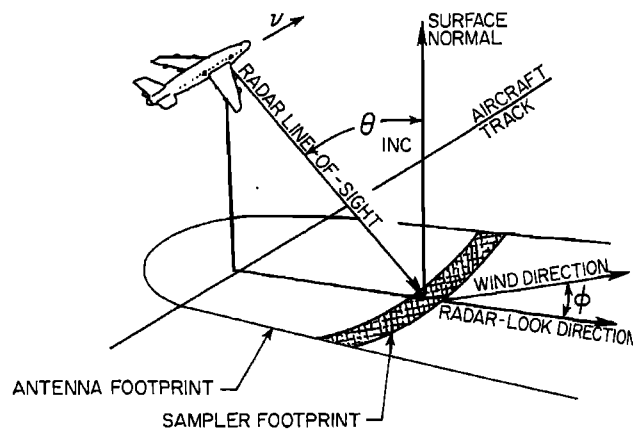


Fig. 2. Geometry for aircraft measurements of L band backscatter from the ocean. All echoes for a given delay were square law detected and recorded on a strip chart. Typical recording parameters were angle of incidence, θ , equal to about 20° . Typical aircraft velocities were 250 m/s. Typical sampler footprints were 0.6 km by 4.0 km.

TABLE 2a. Operating Parameters for JPL L Band, Aircraft SAR Radar

Parameter	Value
Center frequency	1220 MHz
Wavelength	24.6 cm
Pulse length	1.25 μ s
Bandwidth	10 MHz
Time-bandwidth product	12.5
Peak power	4 kw
Antenna azimuth beamwidth	18°
Antenna range beamwidth	90°
Antenna beam center gain	12 dB
Nominal altitude	3 to 12 km
Nominal ground speed	400–500 knots
Nominal pulse frequency	1000 pps at 500 knots

SEASAT-1 SAR operated. Our results may provide a base for determining small-scale difference in surface stress by using SEASAT SAR and scatterometer data. Also, our results will, it is hoped, provide a basis for measuring wind stress from future SAR observations of the oceans.

INSTRUMENTATION

As mentioned above, the L band scatterometer observations reported here were provided by either SEASAT-1 or Marineland Experiment aircraft observations. Wind speeds and directions for the SEASAT-1 observations were provided by simultaneous SEASAT scatterometer measurements. Wind speeds and directions for the aircraft measurements were obtained with surface anemometers deployed on a variety of ships, buoys, and near-shore installations. Although details of these measurements are provided by previous reports by Weissman *et al.* [1980] and Thompson *et al.* [1981, 1982], some discussion of our instrumentation and data reduction is pertinent here.

An overview of the SEASAT-1 instrument geometries is provided by Figure 1 and Table 1. L band radar backscatter values were derived by densitometer measurements of film transparencies of SAR images. In particular, backscatter coefficients were derived every 10 s for seven equally spaced points across the swath. These points correspond to locations on the ocean surface separated by 12.5 km across the SAR swath (perpendicular to the spacecraft track) and by about 66 km along the swath (parallel to the spacecraft track). Backscatter coefficients across the swath were averaged to form a string of backscatter coefficients separated by about 66 km along the track. The conversion of film densities to radar backscatter values are described by Huneycutt [1979] and Thompson [1980]. The algorithms used to convert film density to radar cross section yielded estimates of absolute backscatter coefficients, which had errors up to 3 dB. We have bypassed this issue by considering only changes in the backscatter coefficient, which are designated by the term $\Delta\sigma^0$. Measured values with 66 km separations show little (<0.1 dB) difference; however, backscatter values separated by a few hundred kilometers show significant trends of a few decibels. Thus, we estimated only the *a* and *b* coefficients of equation (1).

These slowly varying trends in radar cross sections were compared with SEASAT scatterometer measurements of surface winds and directions. The SEASAT SAR swath has a width of 100 km centered about 300 km to the right of the spacecraft track. This SAR swath is imbedded in the scatterometer swath, which has a width of 500 km centered about

450 km off the spacecraft track. The scatterometer yields wind speeds and directions for 25 km in both the cross-track and along-track directions. The SEASAT-1 scatterometer generally yields four wind directions at each surface cell, and one of these directions must be selected for comparison with the SAR. Here, a most probable wind direction was selected from circulation models or weather maps provided by the National Weather Service. In addition, the four wind-speed values within the SAR swath were averaged; these averaged wind-speed values were plotted versus position along track for comparison with the SAR backscatter values.

Aircraft measurements provide additional data for testing the relationship between surface stress and L band backscatter from the ocean. We used data obtained during the Marineland Experiment in December 1975, when the NASA CV990 aircraft was equipped with an L band SAR and flew over a number of instrumented sites in the Atlantic Ocean off Marineland, Florida [see Shemdin *et al.*, 1980; Thompson, 1976]. Here, L band backscatter from the ocean was measured by recording an envelope detection of the raw SAR signal at a fixed delay beyond the nadir echo. These were recorded on a strip chart, where echo power could be measured directly. The combination of the antenna pattern and pulse length yielded a footprint of 0.5 km \times 4 km, approximately parallel to the aircraft track as shown in Figure 2. (Radar parameters are given in Table 2.) Surface winds are continuously measured by a number of anemometers on ships, buoys, and on the shore.

The Marineland data are important here since they provide measurements of echo power at a number of angles with respect to the wind. This was accomplished by aircraft flights along short legs in the directions shown in Figure 3. Each leg was flown in about 3 min, aircraft maneuvering between turns normally consumed 7 min more. The entire five-sided and eight-sided patterns were normally flown in 50 and 80 min, respectively.

WIND-RADAR COMPARISON DATA

As described above, L band backscatter from the ocean was measured in two different ways: SEASAT-1 observations provided simultaneous measurement of L band backscatter and K_u band scatterometer-inferred surface winds. Aircraft measurements provided L band scatter measurements at a number of different angles near instrumented surface sites. The data from these two different measurements will be presented here by using different types of plots. Figure 4 provides an overview of SEASAT-1 data analysis.

The SEASAT-1 measurements are given by plots of L

TABLE 2b. Typical Values for the Strip Chart Scatterometer

Parameter	Value
Altitude	12 km (40,000 ft)
Angle of incidence	20°
Range	12.8 km
Azimuth beamwidth	18°
Transmitter pulse length	1.25 μ s
Azimuth (along-track)	4.0 km
Footprint length	
Range (cross-track)	0.55 km
Footprint length	
Antenna gain at beam center ($\theta = 45$ deg)	12.0 dB
Antenna gain at $\theta = 20$ deg	10.5 dB

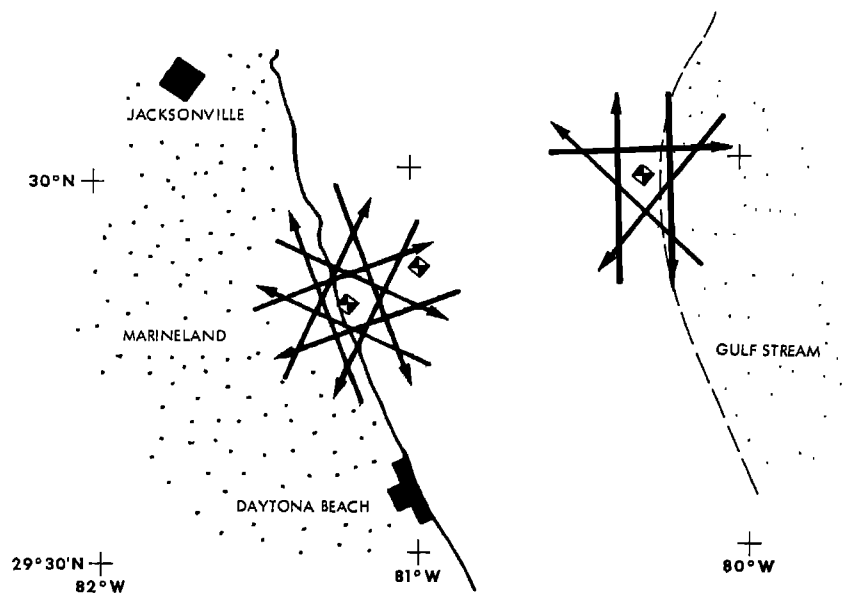


Fig. 3. Flight paths for the eight-sided and five-sided patterns during the Marineland Experiment [see Thompson, 1976; Shemdin, 1980]. The three instrumented sea-surface sites are indicated by the diamonds.

band backscatter and scatterometer winds versus distances along various swaths as shown in Figures 5, 6, and 7. Radar cross section is given in decibels, and the wind direction plots show the upwind (UW), crosswind (CW), and downwind (DW) directions. Distances along the SAR swath are given in terms of latitude at the center of the SAR swath.

The SEASAT-1 data show that L band backscatter generally rises and falls in unison with the wind. Higher L band backscatter values are associated with higher wind speeds and vice versa. To investigate this further, least squares fits were performed on $[\Delta\sigma^0/(1 - b \cos(2\phi))]_{\text{db}}$ versus $|U|_{\text{db}}$ for a number of b values between zero and 0.25. In essence, we investigated $\Delta\sigma^0$ versus $|U|$ on a log-log plot similar to that shown in Figure 8. Each fit as function of b yields an rms error ϵ and a correlation coefficient C given in Table 3. In the case of orbit 1255, there is so little wind variation that the rms error and correlation coefficient vary little with the b parameter. In two other cases (orbits 1126 and 1255), there is a large change with wind direction. Here, the rms error increases monotonically, and the correlation coefficient decreases monotonically with the value of b . The results of these least square fits suggest that a is 0.5 ± 0.1 and b is small ($b = 0.05 \pm 0.05$).

Aircraft measurements during the Marineland Experiment provide another means of determining the wind-direction factor b . Here we have plotted backscattered power (P_{ave}) versus $\cos(2\phi)$ as shown in Figures 9 and 10. The tacit assumption here is that the wind speed is constant over the few tens of minutes that the surface sites were overflown. The vertical bars on the power in the plots indicate the minima and maxima in the observed power. Also, the backscattered power is not calibrated in absolute units.

The Marineland data show two distinct behaviors. All data except that for December 10, 1975, show little, if any, modulation of the echo power with wind or ocean wave direction. Typical data are shown in Figure 9, which shows the eight-sided patterns flown on December 14 and 15, 1975. All Marineland data for December 6, 8, 14, and 15, 1975, suggest that b is nearly zero as shown in Table 4. Some small modulation in echo power may be attributed to wind-speed

changes from land breezes which would be expected at the sites during the time of day that the measurements were made.

In contrast, backscatter for the five-sided pattern on December 10, 1975, shown in Figure 10 has a strong dependence upon the wind direction. Here, we have plotted relative power on and off the Gulf Stream on separate plots since echoes from the Gulf Stream were consistently higher than those off the Gulf Stream. These radar echoes show a strong directional dependence where $b = 0.20 \pm 0.05$. The observations for December 10, 1975, were made during meteorological conditions which were distinctly different than those of the other days of the Marineland Experiment. A cold front had passed through the Marineland area on December 9, 1975, and on December 10, 1975, there was a moderate cold wind out of the northwest blowing across the warm near-shore and Gulf Stream waters. The air was 10°C colder than the water which created an unstable marine boundary layer.

We believe that this unstable atmosphere produced SAR

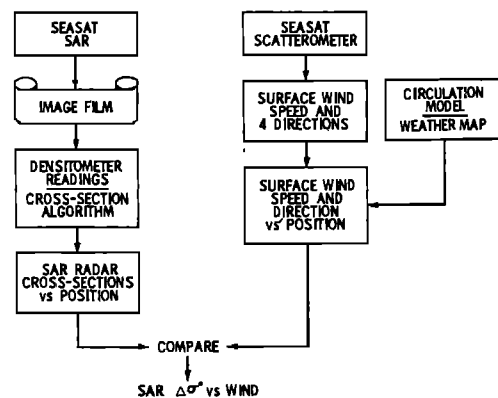


Fig. 4. Overview of SEASAT SAR-scatterometer comparisons. SAR radar cross sections were derived from densitometer measurements of SAR image transparencies [see Thompson, 1980]. The SEASAT scatterometer provided estimates of surface wind magnitudes and directions. Circulation models or weather maps were used to select the most probable wind direction.

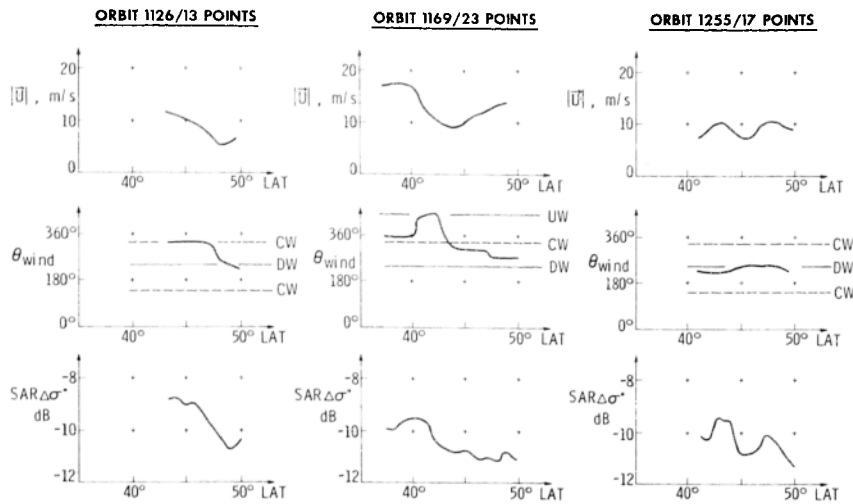


Fig. 5. SEASAT scatterometer wind speed ($|\bar{U}|$), wind direction (θ_{wind}), relative SAR backscatter coefficient ($\Delta\sigma^0$) versus position along tracks for GOASEX, the Gulf of Alaska Experiment. See Figure 6 for track geometries. Wind directions corresponding to crosswind (CW), downwind (DW), and upwind (UW) are indicated.

images on December 10 which are quite different from the SAR images obtained during the other days of the Marineland Experiment. In particular, the SAR images for December 10, 1975, as shown in Figure 11 are characterized by radar-bright splotches, which are several kilometers across and appear strongest when the radar is looking upwind and downwind. They disappear when the radar is looking crosswind. These splotches may be the surface expressions of thermally induced plumes in the boundary layer since they occur simultaneously with kilometer sized cumulus clouds [Thompson *et al.*, 1982]. It appears that the small (25 cm wavelength) gravity waves under these plumes form preferentially in the direction of the mean wind.

Thus, the data for the Marineland Experiment suggest that the wind coefficient b of equation (1) may have a dependence on both the stability of the marine boundary layer and possibly upon wind speed magnitudes. One should recall here that a L band b coefficient of 0.5 was reported by Weissman *et al.* [1979] for the high winds associated with Hurricane Gloria.

SCATTERING MECHANISMS AND RELATIONSHIPS

An overall goal of these wind-backscatter studies is to provide a basis for estimating surface wind and wave conditions from radar backscatter measurements. Here, we have considered how surface winds might be estimated from relative changes in radar backscatter through the empirical relationship given in equation (1). That empirical relation-

ship, which provides the basis for estimating surface winds with K_u band scatterometry, also appears to work for L band backscatter at angles of incidence near 20° where the SEASAT SAR operated. Future spacecraft SAR's may operate at other wavelengths and angles of incidence. Thus, it is important to understand the physical mechanisms that control the radar backscatter.

The basis for relating radar backscatter to surface winds is the close coupling between the short gravity waves and surface wind stress. Radar backscatter is controlled primarily by the number of ocean wavelength at the Bragg wavelength, where the ocean wavelength equals the [radar wavelength/2 sin (angle of incidence)]. The Bragg wavelength for our data is 30 cm, assuming a nominal angle of incidence of 23° and the SEASAT SAR radar wavelength of 23.5 cm. The number of ocean waves at the wavelength grows with surface wind speed, providing the basis for the dependence of radar cross section with wind-speed magnitude. However, the dependence of radar cross section with wind direction requires other effects. Since the azimuthal variation of the short gravity waves is small at lower wind speeds (below the threshold of wave breaking), one expects the slopes of larger wave to be the primary source of azimuthal variations in radar cross section. [See Brown, 1978; Valenzuela, 1978; Moore and Fung, 1979.]

The hypothesis that large slopes generate azimuthal variations in radar cross section can be investigated via model computations. We assume that the large-scale waves have a

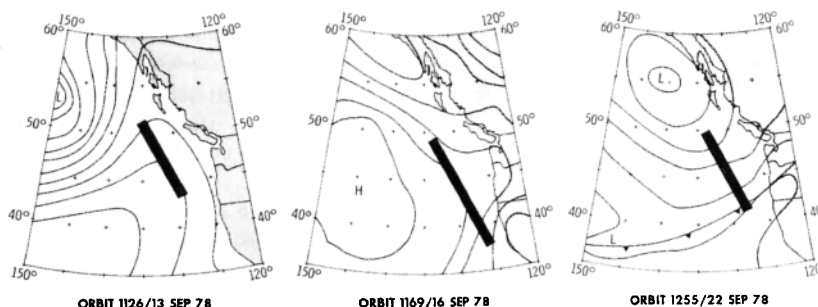


Fig. 6. SEASAT SAR data acquisitions for GOASEX, the Gulf of Alaska Experiment. The SAR swath width of 100 km is shown to scale. Surface pressure analyses were provided by the National Weather Service.

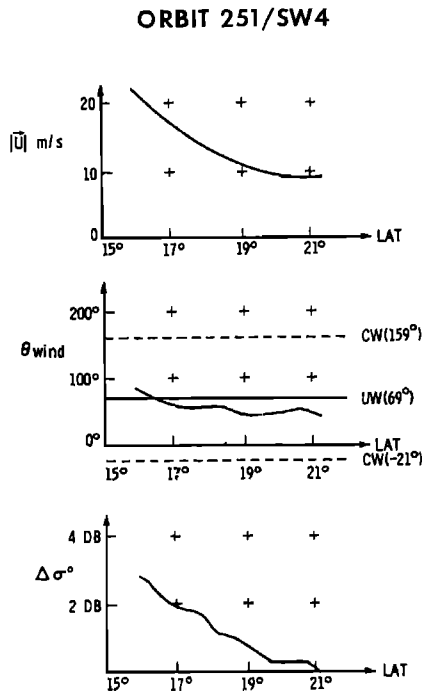


Fig. 7. SEASAT scatterometer wind speeds ($|\vec{U}|$) and direction (θ_{wind}), relative SAR backscatter ($\Delta\sigma^0$) versus position along track for the fourth swath of SEASAT orbit 251. These observations near the eye of hurricane Fico show a drop in relative L band backscatter when wind speeds dropped from 20 to 10 m/s.

cutoff in wavelength ($2\pi/k_c$) of 2 m since Bragg waves can be tilted only by waves that are at least 6 times their length. At wind speeds below about 5 m/s, there is little, if any, azimuthal variation in the radar backscatter. This implies that the mean square upwind and downwind slopes are equal

ORBIT 251/SW4

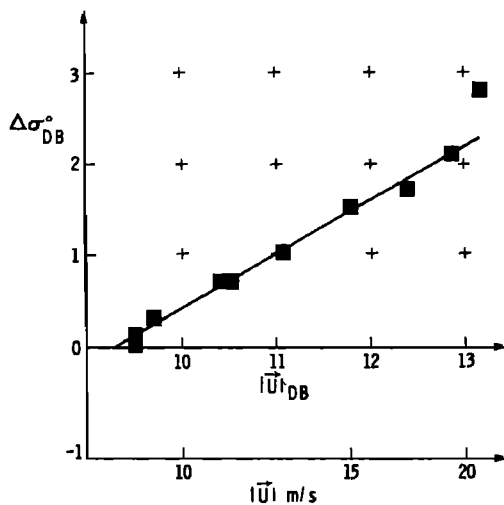


Fig. 8. Log-log plot of SEASAT SAR relative backscatter ($\Delta\sigma^0$) versus scatterometer surface wind speed ($|\vec{U}|$) for SEASAT observations of Hurricane Fico (orbit 251). Both $\Delta\sigma^0$ and ($|\vec{U}|$) are given in decibels.

TABLE 3. Least Square Fit Parameters

Orbit	a	b	Corr. Coef.	rms Diff.
1126	0.519	0.00	0.991	0.114
	0.544	0.05	0.987	0.259
	0.569	0.10	0.981	0.422
	0.594	0.15	0.975	0.590
	0.619	0.20	0.969	0.761
1169	0.477	0.00	0.736	0.412
	0.466	0.05	0.761	0.408
	0.455	0.10	0.740	0.446
	0.444	0.15	0.692	0.517
	0.432	0.20	0.635	0.611
1255	0.518	0.00	0.459	0.487
	0.519	0.05	0.456	0.492
	0.520	0.10	0.453	0.498
	0.521	0.15	0.451	0.503
	0.521	0.20	0.448	0.508

for that part of the ocean wave spectra between 0 and k_c . This wavelength regime is different from the 'clean sea' model of Cox and Munk [1954]. Instead, this regime corresponds to their "oil slick" model. This can be examined further by buoy data since small buoys 'follow the wave surface for wavelengths greater than twice its own diameter' [Stewart, 1980]. We examined the slope spectra reported by Tyler et al. [1974] who obtained upwind-to-crosswind slope ratios of 1.00 ± 0.10 . These ratios are close to those obtained by Cox and Munk for their 'oil slick' observations. These ratios suggest that there will be small differences between the upwind and crosswind radar cross sections which are observed for the lower wind speeds.

Although the upwind-to-crosswind slope ratios near unity provide an explanation for the cases where there is little azimuthal variation in the radar backscatter, we need some other explanation for the significant azimuthal variation observed in the unusual Marineland observation. Our data and others [Keller and Plant, 1979] indicate that higher backscatter powers and significant azimuthal variations when the ocean surface is subjected to an unstable atmosphere from large air-sea temperature differences. Here, the roles of short wave spectra growth, large wave slopes and modulation effects from coupled shear flow [Wright et al., 1980] are not known well enough to mathematically predict changes in radar backscatter. Clearly, more work is needed to model accurately these unstable atmosphere cases.

The discussion of physical mechanisms to this point has concentrated on lower winds where wavebreaking can be ignored. However, at higher winds wave breaking will be important. This may help explain why one aircraft observation of radar backscatter in the eyewall of Hurricane Gloria reported by Weissman et al. [1979] has a large dependence upon wind direction. When wave breaking occurs, it is not clear whether the two-scale scattering model has validity or whether the directional effects depend upon the small-scale spectrum or the large scale slopes. Wave breaking occurs when the orbital velocity (U) exceeds the phase velocity (C) of the wave. Kinsman [1965, p. 271] indicates that the ratio (U/C) equals the product of peak wave height (h) and wave number (k). This implies that when waves break, the product $kh \geq 1$. However, the electromagnetic scattering theories based on perturbation method [Wright, 1966, 1968] require that the product $kh \ll 1$. Thus, these electromagnetic

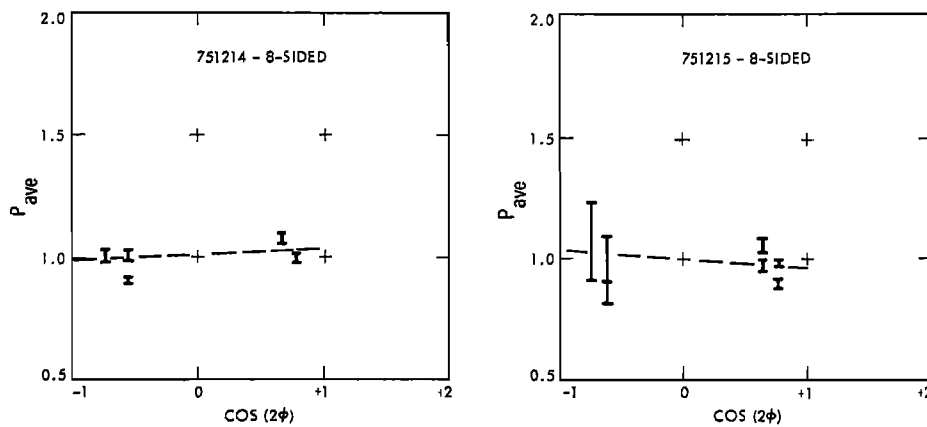


Fig. 9. Marineland Experiment aircraft observations of relative *L* band backscatter power at a 20° angle of incidence versus $\cos(2\phi)$. Angle ϕ is the angle between radar look direction and the wind angle as shown in Figure 2. Note there is no apparent change in power with the surface wind direction. This is typical of all Marineland data except December 10, 1975, which is shown in Figure 10.

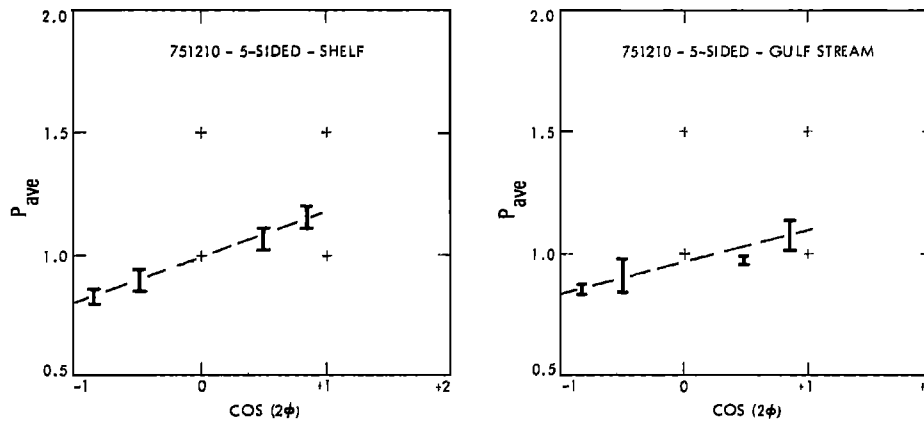


Fig. 10. Marineland Experiment aircraft observations relative *L* band backscatter power at 20° angle of incidence versus $\cos(2\phi)$ for the five-sided pattern for December 10, 1975. These shelf waters had distinctly lower cross sections than the Gulf Stream waters. Thus, the backscatter from these two different types of ocean surfaces are plotted separately. Note the strong dependence of backscatter upon the wind-radar angle, ϕ , in contrast to the lack of wind direction dependence shown in Figure 9. The ocean surface for December 10, 1975, was subjected to higher winds and an unstable marine boundary layer in contrast to lower winds and stable marine boundary layer for the other days of the Marineland Experiment.

theories may not be applicable to the higher wind cases where wave breaking occurs.

In summary, the understanding of ocean surface conditions from radar backscatter measurements requires a two-scale model where radar echo modulations are controlled by both the number of Bragg ocean wavelengths and slopes from the larger wavelengths. The growth of echo power with wind magnitude appears to be well understood. However, the modulation of *L* band backscatter power with wind direction needs further study. Low wind, stable marine

boundary layer cases appear to agree with estimates provided by ratios of upwind-to-crosswind slopes. However, observations of unstable atmospheres with moderate winds and high winds with wave breaking require further theoretical developments.

CONCLUDING REMARKS

Today, there is ample evidence that *L* band backscatter from the ocean is modulated by surface winds. In particular, *L* band backscatter at 25 cm wavelength and near 20° angle

TABLE 4. Summary Marineland Five-Sided and Eight-Sided Pattern Results

Date/Pattern	<i>b</i>	rms Error	θ wind	$ U $, m/s
751204/five-sided	-0.008	0.074	60°	4.5
751206/eight-sided	-0.007	0.146	80°	2.0
751206/five-sided	—	—	—	0
751210/five-sided*	0.144/0.203*	0.038/0.010*	300°	10.0
751214/eight-sided	0.033	0.059	90°	4.0
751214/five-sided*	0.013/-0.031*	0.043/0.014*	90°	3.0
751215/eight-sided	-0.034	0.050	140°	5.0

*Higher Gulf Stream backscatter analyzed separately from lower shelf backscatter.

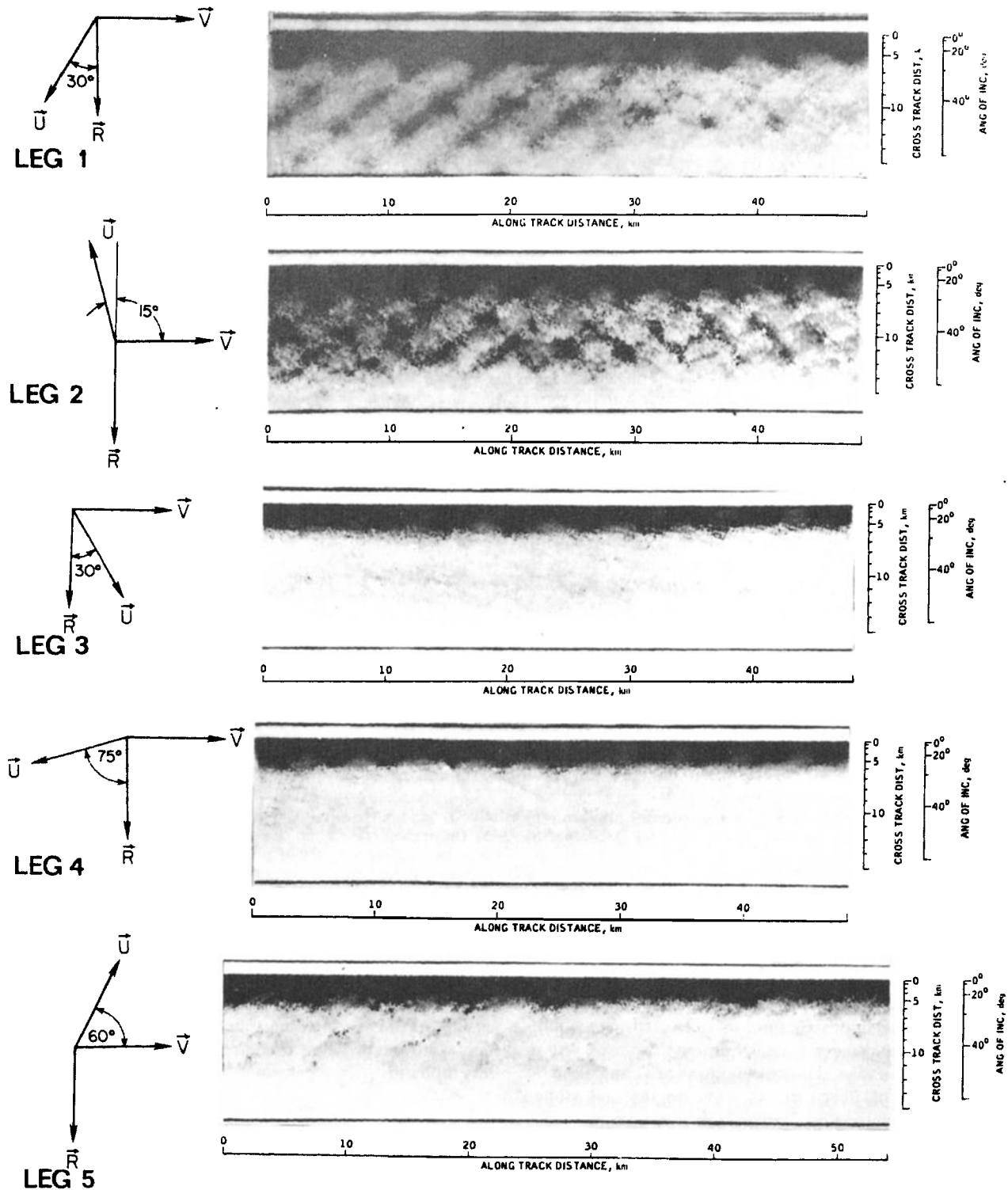


Fig. 11. Aircraft SAR images for the five-sided pattern of December 10, 1975. The line drawings on the left indicate the wind direction (\bar{U} = 10 m/s at 330°), radar look direction (\bar{R}), and the aircraft velocity (\bar{V}). Negative SAR images are used, where radar bright areas are darker. Note the most intense splotches (the darkest areas) occur on leg 2 when the radar is looking nearly upwind, while no splotches occur on leg 4 when radar is looking nearly cross wind. Radar tracks for this five-sided pattern are shown in Figure 3.

of incidence is proportional to (wind speed) $^{0.5 \pm 0.1}$. In contrast, K_u backscatter at 2.2 cm wavelength and near 20° angle of incidence is proportional to (wind speed) $^{1.0 \pm 0.1}$. In addition, K_u backscatter at higher angles of incidence shows an even stronger dependence upon wind speed, approaching (wind speed) $^{2.0}$. L band backscatter from the ocean at higher angles of incidence will have a stronger dependence upon

wind speed than what we measured here near 20° angle of incidence.

Although the dependence of L band backscatter upon wind speed is relatively certain, there is some uncertainty in the wind direction coefficient. Most Marineland and SEA-SAT cases suggest that the wind coefficient b is small (i.e., $0 \leq b \leq 0.1$). However, one Marineland observation of

unstable atmospheric conditions indicates strong wind coefficient, where $b = 0.20 \pm 0.05$. Also, earlier work involving aircraft observations of Hurricane Gloria reported by Weissman et al. [1979] suggest that b for high wind cases may be as large as 0.5. This suggests that the wind coefficient b of equation (1) increases with both wind speed magnitude and boundary layer instability. Clearly, more research is needed to understand how various physical processes control the wind-direction dependence of radar scatter from the ocean.

We have emphasized an empirical approach here by taking existing L band data and fitting it to a mathematical form which had been developed to describe the dependence of K_u band backscatter upon surface winds. The results are encouraging, but numerical comparisons between existing theories, involving surface spectrum models [such as Pierson and Stacy, 1973] still needs to be done. It would be a significant achievement to have a theory which describes both L band and K_u band backscatter in terms of surface wave spectra and wind, and which would also permit estimation of wind speeds at intermediate frequencies where future SARs may operate.

Although current data and its analysis does not permit a complete story, there is enough evidence to indicate that radar backscatter at L band provides surface wind speed measurements. This suggests that SEASAT SAR images in conjunction with the SASS K_u band observations can provide maps of surface wind with scales down to a few tens of meters. The results to date also suggest that surface winds can be obtained from future SARs, whether these future SARs are at X , C , or L band (approximately 3, 6, or 25 cm wavelengths, respectively). The analysis of NRL four-frequency aircraft radar data by Daley [1973] and Jones and Schroeder [1978] suggest that wind dependencies are maximized at shorter radar wavelengths and higher angles of incidence.

Acknowledgments. This work was funded by the NASA and NOAA SEASAT programs. Part of the research described in this paper (D.E.W. and T.W.T.) was carried out by the Jet Propulsion Laboratory, California Institute of Technology, under contract with the National Aeronautics and Space Administration. Part of the research described here (F.I.G.) was funded by the NOAA Seasat Project. We are indebted to Omar Shemdin and Walter E. Brown, Jr., of the Jet Propulsion Laboratory for their encouragement of this study. We are also indebted to two anonymous reviewers for their helpful comments.

REFERENCES

- Barrick, D. E., and C. T. Swift, The SEASAT microwave instruments in historical perspective, *IEEE J. Oceanic Eng.*, 5, 74–79, 1980.
- Beal, R. C., The SEASAT SAR wind and ocean wave monitoring capabilities: A case study for pass 1339M, 28 September 1978, Rep. SIR 79-U019, Johns Hopkins Univ./Applied Phys. Lab., Baltimore, Md., 1979.
- Bracalente, E. M., D. H. Boggs, W. C. Grantham, and J. L. Sweet, The SASS scattering coefficient algorithm, *IEEE J. Oceanic Eng.*, 5, 145–154, 1980.
- Brown, G. S., Backscattering from a Gaussian-distributed perfectly conducting rough surface, *IEEE Trans. Antennas Propagat.*, AP-26, 472–482, 1978.
- Chan, H. L., and A. K. Fung, A theory of sea scatter at large incidence angles, *J. Geophys. Res.*, 82, 3439–3444, 1977.
- Cox, C. S., and W. H. Munk, Statistics of the sea surface derived from sun glitter, *J. Mar. Res.*, 13, 198–227, 1954.
- Daley, J. C., Wind dependence of radar sea return, *J. Geophys. Res.*, 78, 7823–7833, 1973.
- Huneycutt, B., Amplitude calibration for SEASAT-A optically processed data, Internal Document, Jet Propulsion Lab., Pasadena, Calif., 1979.
- Johnson, J. W., L. Williams, E. M. Bracalente, W. L. Grantham, and F. B. Beck, SEASAT-A satellite scatterometer instrument evaluation, *IEEE J. Oceanic Eng.*, 5, 138–144, 1980.
- Jones, W. L., and L. C. Schroeder, Radar backscatter from the ocean: Dependence on surface friction velocity, *Boundary Layer Meteorol.*, 13, 133–149, 1978.
- Jones, W. L., V. E. Delnore, and E. M. Bracalente, The study of mesoscale ocean winds, in *Spaceborne Synthetic Aperture Radar for Oceanography*, edited by R. C. Beal et al., pp. 87–97, The Johns Hopkins University Press, Baltimore, Md., 1981.
- Keller, W. C., and W. J. Plant, Air-sea temperature difference effects in microwave scattering, Abstract, paper presented at URSI Spring Meeting, Univ. of Wash., Seattle, 1979.
- Kinsman, B., *Wind Waves: Their Generation and Propagation on the Ocean Surface*, Prentice-Hall, Englewood Cliffs, N. J., 1965.
- Moore, R. K., and A. K. Fung, Radar determination of winds at sea, *Proc. IEEE*, 67, 1509–1521, 1979.
- Pierson, W. J., and R. A. Stacy, The elevation, slope, and curvature spectra of a wind roughened sea surface, *NASA CR-2247*, Washington, D. C., Dec. 1973.
- Ross, D. B., The wind speed dependency of ocean microwave backscatter, in *Spaceborne Synthetic Aperture Radar for Oceanography*, edited by R. C. Beal et al., pp. 75–86, The Johns Hopkins University Press, Baltimore, Md., 1981.
- Schroeder, L. C., W. L. Grantham, J. L. Mitchell, and J. L. Sweet, SASS measurements of the K_u -band radar signature of the ocean, *IEEE J. Oceanic Eng.*, 7, 3–14, 1982.
- Shemdin, O. H., The Marineland Experiment: An overview, *Eos*, 61, 625–626, 1980.
- Stewart, R. H., Ocean wave measuring techniques, in *Air-Sea Interaction: Instruments and Methods*, edited by F. Dobson, L. Hasse, and R. Davis, Plenum, New York, 1980.
- Thompson, T. W., JPL radar operations: Marineland-GASP test series, 25 November to 16 December 1975, *JPL Doc. 622-13*, Jet Propulsion Lab., Pasadena, Calif., 1976.
- Thompson, T. W., SEASAT-1 SAR amplitude calibration, *Rep. J-142-917-TI*, Science Applications, Inc., Pasadena, Calif., 1980.
- Thompson, T. W., D. E. Weissman, and F. I. Gonzalez, Seasat SAR cross-section modulation by surface winds: GOASEX observations, *Geophys. Res. Lett.*, 8, 159–162, 1981.
- Thompson, T. W., D. E. Weissman, and W. T. Liu, Marineland aircraft observations of L -band radar backscatter dependence upon wind direction, in *Proceedings of IUCRM Symposium: Wave Dynamics and Radio Probing of the Ocean Surface*, Plenum, New York, 1982.
- Tyler, G. L., C. C. Teague, R. H. Stewart, A. M. Peterson, W. H. Munk, and J. W. Joy, Wave directional spectra from synthetic aperture observations of radio scatter, *Deep Sea Res.*, 2, 989–1016, 1974.
- Valenzuela, G. R., Theories for the interaction of electromagnetic and oceanic waves—A review, *Boundary Layer Meteorol.*, 13, 133–149, 1978.
- Weissman, D. E., and T. W. Thompson, Detection and interpretation of ocean roughness variations across the Gulf Stream inferred from radar cross section observations, *Oceans '77 Conf. Rec.*, 1, 14B1–14B10, 1977.
- Weissman, D. E., D. B. King, and T. W. Thompson, Relationship between hurricane surface winds and L -band radar backscatter from the sea surface, *J. Appl. Meteorol.*, 18(8), 1023–1034, 1979.
- Weissman, D. E., T. W. Thompson, and R. Legeckis, Modulation of sea surface radar cross-section by surface stress: Wind speed and temperature effects across the Gulf Stream, *J. Geophys. Res.*, 85, 5032–5042, 1980.
- Wright, J. W., Backscattering from capillary waves with application to sea clutter, *IEEE Trans. Antennas Propagat.*, 14, 749–754, 1966.
- Wright, J. W., A new model for sea clutter, *IEEE Trans. Antennas and Propagat.*, 16, 217–223, 1968.
- Wright, J. W., W. J. Plant, W. C. Keller, and W. L. Jones, Ocean wave-radar modulation transfer functions from the West Coast Experiment, *J. Geophys. Res.*, 85, 4957–4966, 1980.

(Received November 2, 1981;
revised April 28, 1982;
accepted April 28, 1982.)